Please cite this article in press as: Lee et al., Organic electronic synapses with low energy consumption, Joule (2021), https://doi.org/10.1016/j.joule.2021.01.005

Joule

CellPress

Perspective

Organic electronic synapses with low energy consumption

Yeongjun Lee,[1,5] Hea-Lim Park,[1,5] Yeongin Kim,[2] and Tae-Woo Lee[1,3,4,*]

SUMMARY

The von Neumann computing architecture consists of separated processing and memory elements; it is too bulky and energy-intensive to be implemented in the upcoming artificial intelligence age. In contrast, neurons and synapses in a brain perform learning and memory in an integrated manner and function energy-efficiently by analog adjustment of synaptic strengths in response to stimulation. Organic artificial synapses provide good emulation of the functions and structures of biological synapses and are easily fabricated and therefore can be applied to various neuromorphic electronic devices. In particular, organic artificial synapses that consume energy at a level comparable to that of a biological synapse show great promise for use in future low-energy neuromorphic devices. Here, we review the trends of energy consumption of organic artificial synapses and how it is affected by the structure, materials, and operation mechanism. We also present a strategy to decrease the energy consumption of organic neuromorphic devices. Our review will help the development of versatile low-energy organic neuromorphic electronics.

INTRODUCTION

The biological neural networks in a human brain have a massively parallel configuration of $\sim 10^{12}$ neurons and $\sim 10^{15}$ synapses in <2 L of space with a weight of 1 kg and operate at low power of <20 W.[1,2] These characteristics are superior to those of the conventional von Neumann architecture that have difficulties in demonstrating the future artificial intelligence (AI) due to bulky and rigid structures (e.g., IBM Summit has ~10,000 CPUs and ~27,000 GPUs in 520 m^2 with a weight of 340 tons), a huge power requirement (>15 MW), and serial connection of computing cells and memory cells through buses, which increase energy use and limit computation speed.[3] Also, a human brain efficiently executes memory and recognition processes at extremely small energy consumption E (10 fJ/synaptic event).[4,5] Therefore, neuromorphic electronics that emulate a biological neuronal system are well suited for use in next-generation computing, machines, and AI (Figure 1).

Neuromorphic electronic devices emulate the structures and functions of biological neurons and synapses, which are the main components of biological nervous systems. They generate neural signals and transmit them through a body. The process exploits synaptic plasticity to achieve various responses.[6–9] In a conventional design in which a central processor controls separated sensing and reading units, each pixel must be periodically read out through control and readout circuits even when input is absent, so a certain amount of standby energy is continuously dissipated.[10–12] For example, state-of-art microprocessors are composed of $\sim 10^9$ transistors but input events are intermittent, so an enormous amount of energy is wasted on the periodic

Context & scale

Organic artificial synapses are emerging devices for future neuromorphic electronics that will overcome the high energy consumption and bulky structure of conventional von Neumann computing systems. Event-driven operation of organic artificial synapses is expected to be much more energetically efficient than the clock-rate-type operation of conventional von Neumann processors. Organic synapses have demonstrated spike-dependent synaptic plasticity, which is the basis of learning rules in a brain and of signal transmission in a body; these results have proved the potential of organic artificial synapses for application as core components of future cybernetic electronics and robotics. Organic artificial synapses with diverse device structures, working mechanisms, and materials have demonstrated low energy consumption. In addition, artificial organic peripheral nerves that operate on an event basis can realize robots and neural prostheses that consume energy more efficiently than conventional systems.

In this Perspective, we review the progress of organic artificial synapses, focusing particularly on energy consumption, describing current challenges, and suggesting future research directions for researchers to demonstrate organic artificial synapses with low energy consumption.

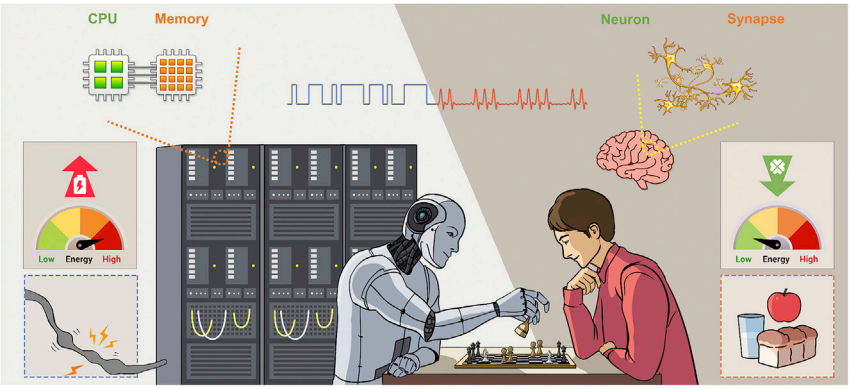

Figure 1. Comparison of high-electric-power von Neumann supercomputing/machine system and an energy-efficient biological system

Use of neuromorphic architecture with artificial synapses to replace conventional systems could improve energy efficiency of electronics and robotics.

scanning of pixels.[13] To increase energy efficiency, neuromorphic electronics should emulate event-driven biological systems, which consume energy only during input events.

By mimicking the biological nervous system, artificial synapses can demonstrate spike-driven brain-inspired computing systems by modulating the synaptic weight according to the delivered neural signals.[14] The synaptic weight is a key parameter to express the strength of a synaptic connection between neurons, which enables spike-timing-dependent control of short-term plasticity and long-term memory states, so event-driven artificial synapses of neuromorphic computing are much more energy efficient than conventional central processors that operate at a fixed clock rate.

Artificial synapses can also emulate afferent/efferent nerves by imitating the mechanism by which sensory and motor nerves transmit signals.[6,7,10,14–20] Advanced bio-inspired soft robots and neural prostheses can be implemented by realizing robots that use a spike neural network, which emulates a body's system that uses action potentials (AC signal). This architecture is superior to the conventional sensors that use DC and robots that use pneumatic activation or are driven by high voltage.[21,22] Use of action potentials can be exploited to generate artificial neural signals from artificial sensory organs and to transfer the signals to the brain, which processes the perceived stimuli.[10,14–20] Especially, artificial synapses can be used to stimulate biological or artificial motor organs to induce appropriate responses.[10,16–18] A neuromorphic system that operates at low power and that emulates a biological neural system would enable development of next-generation brain-inspired computing, bio-inspired robots, and neuro-inspired electronic prostheses and bionics.

The first artificial synapses were constructed using silicon complementary metal-oxide-semiconductor (CMOS) chips and circuit architecture. These artificial synapses emulated signals of biological synapses but each synapse was composed of several transistors.[23–25] Therefore, these silicon CMOS chips have complicated circuit configurations and are fabricated using a hyper-scaling lithography process. They also spend ~10 pJ/synaptic spike (e.g., IBM TrueNorth and Intel Loihi), which is ~10^3-times higher than that of a biological synapse (10 fJ/synaptic event).[4,5,13,26–30] Also, supercomputers that use CMOS circuits (e.g., SpiNNaker, which is a digital system for simulation of neurons and synapses at the software level) also have bulky and

[1]Department of Materials Science and Engineering, Seoul National University, Seoul 08826, Republic of Korea

[2]Department of Mechanical Engineering, Massachusetts Institute of Technology, Cambridge, MA, USA

[3]Nano Systems Institute (NSI), Institute of Engineering Research, Research Institute of Advanced Materials, Seoul National University, Seoul 08826, Republic of Korea

[4]School of Chemical and Biological Engineering, Seoul National University, Seoul 08826, Republic of Korea

[5]These authors contributed equally

*Correspondence: twlees@snu.ac.kr, taewlees@gmail.com

https://doi.org/10.1016/j.joule.2021.01.005

rigid structures (10^6 processor cores and 10^8 transistors in 10 m^3) and high power requirements (several tens of kilowatts).[28–33] Along with efforts to improve operational efficiency, simplify the circuitry, and reduce energy spending in silicon-based synapse, alternative devices with simple geometry and easy operation with two-terminal resistive memory and three-terminal transistors that directly emulate synaptic functions have been developed.[6–8,14,34–36]

Organic artificial synapses are promising candidates for future neuromorphic electronics, because of advantages such as (1) compatibility with solution-printing and micro-patterning lithography processes; (2) easy tunability of molecular, chemical, electrical, and mechanical properties for many purposes; and (3) mechanical flexibility/stretchability with low elastic modulus similar to those of biological neurons. Moreover, in the aspect of the device size, which has an important effect on *E*, organic materials can be patterned to submicron dimension by low-cost solution printing or photolithography[5,37]; such microminiaturized organic synapses can potentially realize low *E*.

Organic artificial synapses that operate with field-driven ion migration can produce sensitive and adaptive synaptic responses to weak stimulation[36,38]; this reaction mimics the responses to neurotransmitters by biological synapses. Therefore, use of organic artificial synapses that consume low energy may yield energy-efficient brain-inspired computing, memory, AI, biomimetic robotic sensory and motor nervous systems, and neural prosthesis that are comparable with a body.

Energy consumption of biological and organic artificial synapses

A biological nervous system is mainly composed of two kinds of synapses: electrical and chemical. Neurons with electrical synapses are almost directly linked to each other with a gap junction of 3.5 nm, which is much shorter than the synaptic cleft (~20–40 nm) of chemical synapse.[39] Electrical synapses can pass nerve impulses directly between the presynaptic membrane and postsynaptic membrane (mostly bidirectional transmission) by electrical coupling, so signal transmission is much faster than in chemical synapses that use neurotransmitters to transfer neural impulses.[39] The simple structure and mechanism of an electrical synapse enables rapid signal transmission but limits synaptic behaviors related to learning and memory.[40] Chemical synapses engage in complicated synaptic activities, can precisely control synaptic strength, and demonstrate various kinds of synaptic plasticity.[39] In a chemical synapse, neurotransmitters diffuse from the presynaptic membrane to the postsynaptic membrane through the synaptic cleft, and the capture of the neurotransmitters by the postsynaptic membrane stimulates the opening of ion channels (Figure 2A). Ions move through the channels; the consequent depolarization of the postneuron elicits an excitatory response, or hyperpolarization elicits an inhibitory response. This procedure consumes 10^9 adenosine triphosphate (ATP) molecules per action potential and 10^5 ATP molecules per synaptic transmission. Each ATP yields 0.1 aJ of energy, so the sum of these usage rates is 100 pJ per action potential and 10 fJ per synaptic transmission.[41] Therefore, a synapse can conduct synaptic activity related to learning and memory by consuming extremely low energy. Artificial synapses are designed to emulate the structure and signal transmission of biological synapses, with the goal of developing neuromorphic electronic devices that consume a similar amount of energy as biological synapses.

Most organic artificial synapses mimic the mechanism of a chemical synapse that uses neurotransmitters. In chemical synapses, synaptic strength is precisely controlled (synaptic plasticity),[7,14] and this ability is very important for neuromorphic

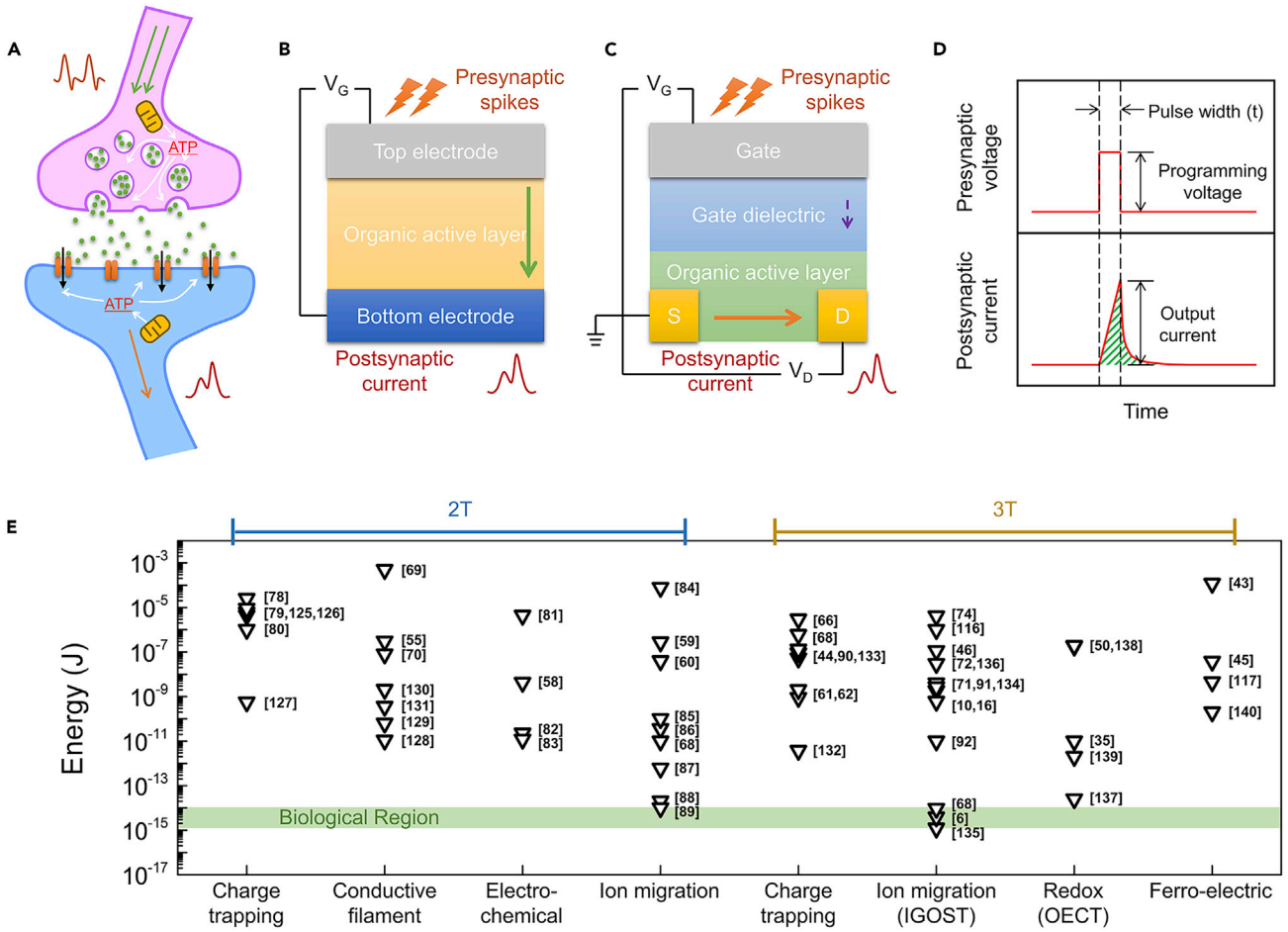

Figure 2. Energy dissipation of organic artificial synapses

(A–C) Schematics of (A) biological synapse, (B) 2-T organic artificial synapse, and (C) 3-T organic artificial synapse.

(D) Schematic of presynaptic voltage pulse and postsynaptic current curves over time; they are used in calculation of energy dissipation.

(E) Energy consumption per synaptic event of organic artificial synapses depending on structures and working mechanisms. *E* of synaptic transistor that uses inorganic material (Indium tungsten oxide) is included for comparison.[42]

electronics. Two-terminal (2-T) and three-terminal (3-T) organic artificial synapses have been reported as basic units of neuromorphic engineering (Figures 2B and 2C).

In a 2-T artificial synapse, one electrode mimics the presynaptic membrane that applies presynaptic impulses; the other electrode mimics the postsynaptic membrane by reading the conductance change of an active layer sandwiched between two electrodes (Figure 2B). The structures of 2-T synapses are similar to that of biological synapses and much simpler than 3-T devices, so when a multipixel synapse array is necessary, the structure and operation would be more straightforward for 2-T devices than for 3-T devices.

In a 3-T artificial synapse, a gate electrode generally applies presynaptic voltage pulses and a drain electrode reads the change in conductance of the active layer (postsynaptic current) between the source and drain electrodes (Figure 2C). A 3-T artificial synapse with multiple gate electrodes or source electrodes receives spatio-temporal information and processes logic operation. External sensory stimuli are additional presynaptic sources to control the synaptic weight of devices. Therefore,

the utility of 3-T devices can be expanded by using them to endow additional functions on multigated synaptic transistors, global-gated synaptic transistors, and stimulus-sensory synaptic transistors.

Power and energy consumption are important characteristics of an artificial synapse. Power consumption P [W] of devices is the product of current I [A] and voltage V [V] as $P = I \times V$. E [J] is the product of V and the integral of the curve of I versus time t [s], to consider the rise and decay of I,[43] but for convenience a simple formula generally considers maximum I and t as $E = P \times t$ (Figure 2D).[5,37]

To calculate the E of an artificial synapse, its operation can be divided into two steps: programming (i.e., writing or switching) and reading. Calculation of the E of the programming step must consider the programming presynaptic voltage. Generally, in 2-T devices, the reading voltage is much smaller than the programming voltage, so programming voltage is a dominant component of voltage. Calculation of P of a 2-T device for the reading step considers only a small reading voltage. However, this calculation for a 3-T device requires partitioning of voltage into gate voltage (V_G) and drain voltage (V_D) and of current into gate current (I_G) and drain current (I_D), as $P = V_G \times I_G + V_D \times I_D$. In systems that are operated with decoupled switching and reading steps or are operated with large V_G or I_G, the gate component ($V_G \times I_G$) should be considered for the calculation of P. In contrast, in many cases, I_G is regarded as dielectric leakage current and metal-oxide-semiconductor (MOS) capacitor charging current and is negligible compared to I_D. Therefore, P in 3-T devices has generally been simplified to $P \sim V_D \times I_D$. Interests in organic neuromorphic electronics are increasing, and E of organic artificial synapses varies widely depending on the device structures and working mechanisms (Figure 2E).[5–10,14–19,34–38; 42,44–80; 81–110] In this perspective, we will review the progress of organic artificial synapses in terms of driving mechanism, materials, device size, and their effects on P and E.

The reported 2-T and 3-T organic synapses exploit similar operation mechanisms (e.g., charge trapping, ion migration, electrochemical reactions, and ferroelectricity) except for a metallic-filament formation mechanism observed only in 2-T devices. Calculated E of organic synapses has been mainly dependent on the operating mechanisms rather than on the device configuration (2-T or 3-T) (Figure 2E). Therefore, we will describe E of a 2-T synapse that uses metallic-filament formation mechanism and E of 3-T synapses that use other mechanisms and materials.

In a 2-T device that uses a metallic-filament mechanism, synaptic memory characteristics exploit resistive switching by formation of a conductive filament.[44–52] Initially, the device has high resistance; applied voltage pulses oxidize the active electrode (e.g., Ag or Cu) and the resulting metal ions migrate to the polymer matrix in which they are reduced to metal nanoparticle clusters that self-assemble to form filament bridges, which are conductive, so the device develops low resistance.[44–51] The conducting path connects both electrodes, so current (microampere to milliampere) and energy dissipation are large. When the electrical stimulus is removed, the filament bridges can gradually be broken by spontaneous rupture due to minimization of interfacial energy or the Gibbs-Thomson effect[46,50] or by electrochemical oxidation of metal filaments when reverse voltage pulses are applied;[45,49,50] in these cases, the device returns to a high resistance state.

The programming voltage of devices varies widely according to device structure and operating mechanism. Artificial synapses that exploit charge trapping in charge-storage

materials usually use charge tunneling or trapping by electric-field-induced charge transport.[53–59] Floating-gated synaptic transistors with charge-storage materials embedded in the insulating layers show synaptic memory responses that exploit field-induced charge tunneling and trapping, which strengthen the local electric field and modulate the threshold voltages of transistors. For example, application of a strong electric field to the control gate electrodes induces hole tunneling from the p-type organic semiconductors (pentacene or dinaphtho[2,3-b:2′,3′-f] thieno[3,2-b]thiophene) to the charge-trapping materials (C_{60} or Al).[53,54] On the contrary, photo-induced excitons of photosensitive materials (perovskite nanoparticles) embedded in the insulating layers of poly(methyl methacrylate) (PMMA) and SiO_2 are dissociated and holes are transferred to the pentacene layer; trapped electrons yield a consequent shift ΔV_{th} in threshold voltage (V_{th}) and an additional internal electric field.[55] Polar groups on the surface of a polymer insulator can also trap photo-induced charge carriers at the interface between an organic semiconductor and a dielectric layer.[60,61] Because of this interfacial charge-trapping effect, electrons from photocarriers of organic semiconductors fill the shallow or deep traps, so excessive holes in the organic semiconductor cause a ΔV_{th}.[60,61]

A ferroelectric copolymer, poly(vinylidenedifluoride-co-trifluoroethylene) (PVDF−TrFE), has been used as a dielectric of the transistor; the dipoles are aligned by the electric field that is caused by V_G and modulate a channel current. Generally, the transfer curve shows a large current hysteresis.[62,63] PVDF-TrFE is widely used in non-volatile bistable memory devices because of its large on/off current margin and stable retention and endurance.[64] In organic ferroelectric synaptic transistors, the presynaptic voltage pulses gradually align the orientation of the dipole.[65,66] Hole accumulation by organic semiconductors can be controlled, so synaptic potentiation and depression can be achieved.[65,66]

These devices are operated by charge transport driven by an electric field, so voltage amplitude is dependent on the capacitance of an insulating layer. To decrease the voltage amplitude, use of high-dielectric-constant insulators would be a superior strategy. For example, high programming voltage pulses (>|10| V) were required to modulate the V_{th} of pentacene/Au nanoparticle (NPs) blended film with SiO_2 dielectric layer by storing field-induced holes from pentacene to the Au NPs.[57,58] Through the use of an aqueous electrolyte dielectric with high electric double layer (EDL) capacitance, the programming voltage spike amplitude was reduced to 50 mV.[59] Blending of ionic liquid with PVDF-TrFE can induce formation of an EDL by ion accumulation and, thereby, reduce the amplitude of the presynaptic voltage pulses from >|10| V in the PVDF-TrFE-only device, to <|2| V.[66,67]

The E of the two mechanisms was compared in a single cell. Synaptic transistors in which the active material is molybdenum disulfide (MoS_2) showed synaptic properties with two modes: electronic mode with a SiO_2 dielectric that exploits interfacial traps and ionotronic mode with an ionic liquid dielectric that exploits an EDL.[68] The electronic mode was operated by a much larger voltage pulse amplitude (−50 V) with higher E (~13 nJ/synaptic event) than the ionotronic mode operation (voltage amplitude = 2 V, calculated E ~4.8 pJ/synaptic event).[68] In a similar device structure in which the active material was indium tungsten oxide, the electronic mode was operated by voltage pulse amplitude (20 V) with higher E ~600 nJ/synaptic event than the ionotronic mode (voltage amplitude = 1.5 V, E ~9.3 fJ/synaptic event) (Figure 3A).[42]

In synaptic transistors that use electrolyte and that have low driving-voltage pulses, the postsynaptic current level varies depending on the conductivity of the pristine active channel materials. For example, poly(3,4-ethylenedioxythiophene):polystyrene sulfonate (PEDOT:PSS) is a conducting polymer that has high pristine conductivity, so

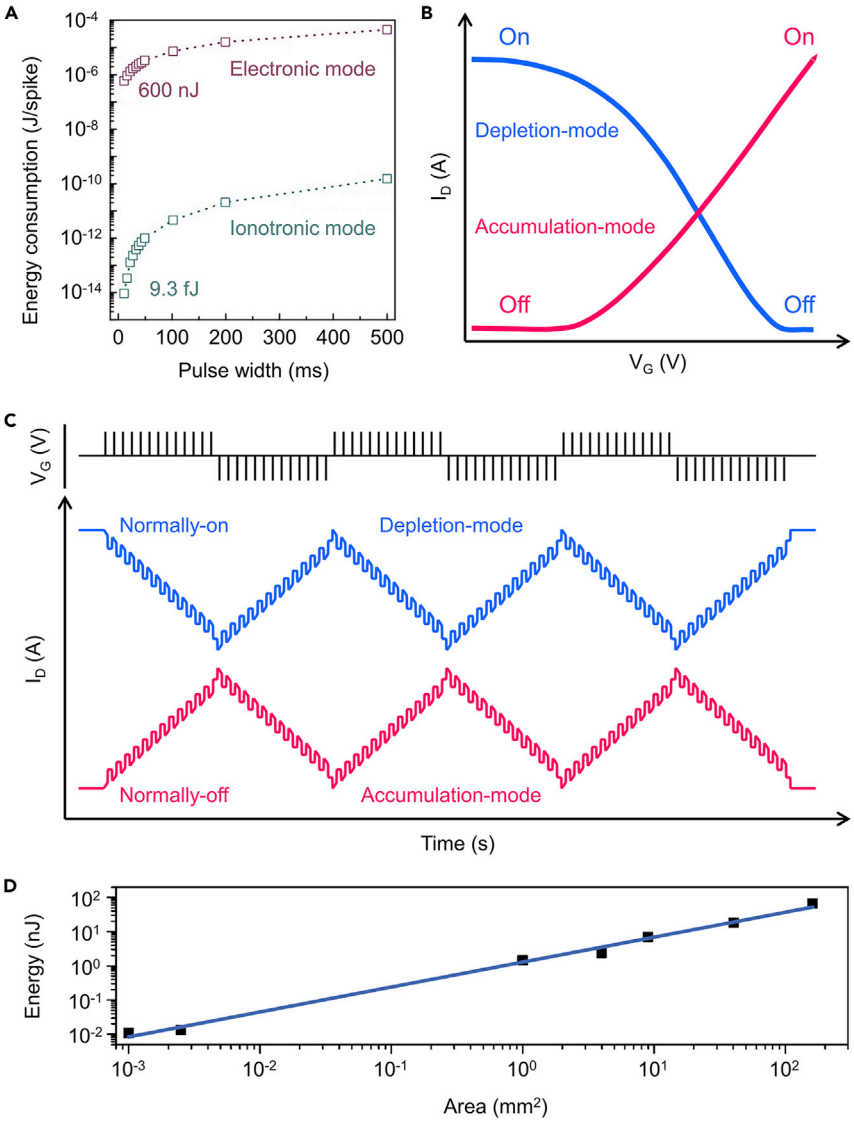

Figure 3. Energy consumption of organic artificial synaptic transistors depending on working mechanisms, materials, and device size

(A) Energy consumption of organic artificial synapse depending on operation modes (ionotronic versus electronic). Reproduced with permission.[42] Copyright 2018, American Chemical Society.

(B and C) Overview of typical operation of (B) drain current-gate voltage (I_D-V_G) curves and (C) drain current (synaptic weight) modulation of electrolyte-based organic artificial synapses with depletion-mode-operated high-conductivity conducting polymer (PEDOT:PSS) and accumulation-mode-operated low-conductivity semiconducting polymer (PBTTT).

(D) Dependence of energy consumption on device size of organic artificial synaptic transistor.

(B–D) Reproduced with permission.[37] Copyright 2017, Nature Publishing Group. Reproduced with permission.[71] Copyright 2018, Wiley-VCH.

electrochemical synaptic transistors that use PEDOT:PSS for a channel showed a high resting current and operated in a depletion mode that lowers the conductivity of PEDOT:PSS according to the presynaptic voltage pulses (0.1 V).[69] A device that has an organic battery-like switching mechanism with PEDOT:PSS for a gate electrode and de-doped PEDOT:PSS by poly(ethylenimine) (PEI) for a channel. Channel conductance is changed by proton (H^+) exchange between the gate, electrolyte, and channel with

very small electrochemical overpotential (|1.5| mV) (Figure 3B).[8,37,70] However, the device is normally in the "ON" state with high current before stimulation, so the *E* is expected to be much higher than normally "OFF" devices that use a semiconducting polymer (Figure 3C).[71]

Poly[2,5-bis(3-tetradecylthiophen-2-yl)thieno[3,2-b]thiophene]) (PBTTT) is a semiconducting material that initially has low conductivity. Organic battery-like synaptic devices that use PBTTT for a channel and PBTTT doped with F4TCNQ (7,7,8,8-tetracyano-2,3,5,6-tetrafluoroquinodimethane) for a gate electrode operate in accumulation mode, which increases channel conductivity when a voltage pulse (|2| mV) is applied (Figures 3B and 3C).[71] Therefore, electrochemical synaptic transistors that use a low-conductivity semiconducting polymer should have lower *E* than the device that uses a high-conductivity polymer, under similar voltages.[37,71]

The output current of a device is generally proportional to its channel area, so *E* can be reduced by minimizing the device size. A battery-like electrochemical synaptic transistor with channel area of 10^{-3} mm^2 and that used PEDOT:PSS/PEI for a channel and PEDOT:PSS for a gate electrode had calculated *E* ~10 pJ, which is projected to be decreased to ~35 aJ in a device that has a channel area of ~10^{-8} mm^2, which can be fabricated by optical lithography (Figure 3D).[8,37] A 300-nm-scale organic synaptic device that consumes energy at the level of the biological synapse (~10 fJ) was fabricated by simple, low cost, and direct nanowire printing,[5] instead of a high-cost, multistep, and slow lithography. These size-dependent, low currents can be exploited to reduce *E*.

Short pulse width can reduce *E* and enable conductance modulation at high speeds. Biological neurons switch on a millisecond scale, whereas electronic devices can be fabricated to switch on microsecond and nanosecond scales, which are advantageous to reduce *E*. In battery-like electrochemical synaptic transistors that use PEDOT:PSS/PEI for a channel and PEDOT:PSS for a gate electrode, a pulse that had a duration of a few milliseconds was used when the synaptic response was induced by ion migration.[37] Simulation suggested that reduction of switching time to <1 μs would be possible with further optimization of the device and the circuit by miniaturizing the device feature size to reduce device capacitance, operating with many conductance states within a small dynamic range and preventing self-discharge of the device with an additional element (a resistor or a selector).[72] The predicted switching *E* and switching time are 170 fJ and 500 ns for a 1 μm × 1 μm × 200 nm (length × width × thickness) channel with 100 conductance states, respectively. The timescale should be matched with the targeted applications; for example, short pulses (~1 μs) are required in electronic devices but may not be necessary for biocompatibility.

ENERGY CONSUMPTION OF ARTIFICIAL SYNAPSES INTEGRATED WITH SENSING/MOTOR ELEMENTS

Artificial synapses integrated with sensing/motor elements or artificial sensory/motor synapses can be developed to mimic the sensing and responding dynamics in biological systems and could be core technologies for soft robotics and neural prosthetics. In biological systems, sensing of stimuli is achieved by afferent nerves, whereas responses with muscles use efferent nerves.

This section addresses the challenge of reducing *E* in artificial synapses integrated with sensing/motor functions and merging synaptic characteristics with biomimetic sensing elements.

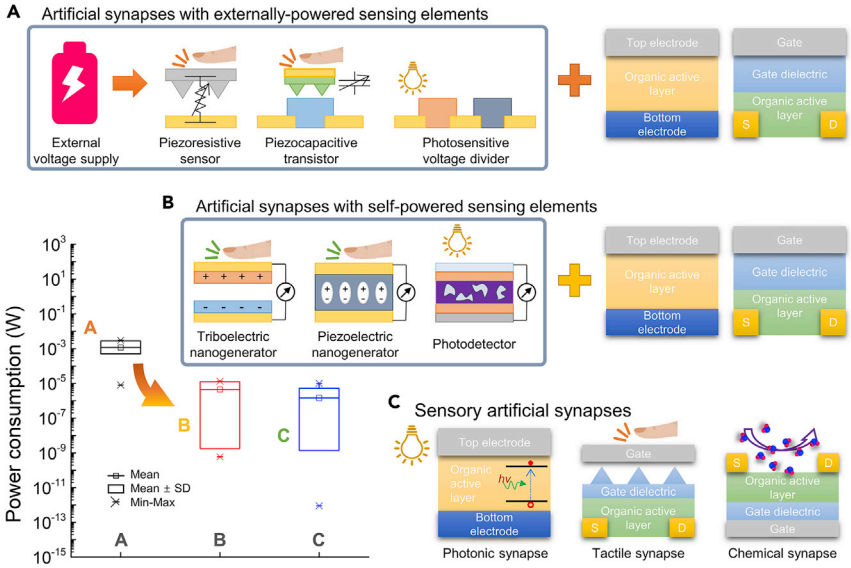

Figure 4. Power comparisons of organic artificial synapses integrated with different sensory elements

(A–C) Schematic diagrams of artificial synapses (A) with externally powered sensing elements and (B) with self-powered sensing elements (a polymer actuator is also connected to demonstrate an artificial motor nerve), and (C) sensory artificial synapses that integrate sensing and synaptic functions in a unit cell.

First, synaptic devices are integrated with sensing elements that are powered by external sources (Figure 4A). For visual perception systems, ferroelectric/electrochemical-modulated artificial synapses were integrated with photosensitive elements and showed a dynamic range of synaptic signals from volatile to non-volatile, depending on incident light intensity, wavelength, and frequency.[65] For artificial tactile perception systems, two organic devices with synaptic and tactile sensing functions were compactly integrated;[73,74,89,101] these tactile perception systems could distinguish English characters after a training process[89] and could memorize signals of "touch" and "hit" at different pressure levels.[73] For a pressure-sensory alarm system, a flexible artificial nociceptor was connected with a piezoresistive sensor.[74] A biological nociceptor's characteristics of threshold, relaxation, allodynia, and hyperalgesia behaviors were mimicked by memristors by exploiting formation and rupture of the Ag filament.[74] 3-T devices, a dual-organic-transistor-based tactile perception element (DOT-TPE) was obtained by combining the gate electrode of the synaptic device with the source of the sensing transistor.[101] This DOT-TPE system could distinguish intensity, frequency, duration, and the number applications of pressure.[101] These systems could process detected information, depending on the external stimuli. However, these systems inevitably had higher E than a single synaptic device because operation of the sensing units requires additional energy.

Typical sensory receptors showed maximum P in the range of milliwatts (transistor type)[110–113] or microwatts (resistive type)[114–116] per sensor but the total P is still huge. Thus, synaptic devices with externally powered sensing elements usually demonstrated average P in the milliwatt range (Figure 4). P of the sensing parts can be further reduced by integrating the artificial synapses with self-powered sensing elements or by using artificial sensory synapses.

Artificial synapses have been combined with self-powered sensors, such as triboelectric, piezoelectric, photovoltaic, and thermoelectric devices (Figure 4B). In these artificial synapses, most of the energy is usually used by synaptic devices. A self-

powered triboelectric nanogenerator (TENG) was used to convert pressure information to voltage pulses without consuming power.[18,99,117] The TENG transferred output voltage pulses to the artificial synapse, which demonstrated various kinds of synaptic plasticity such as paired-pulse facilitation, spike-number-dependent plasticity, and spike-rate-dependent plasticity.[99] A self-powered photodetector (PD) has been used to demonstrate an optoelectronic sensorimotor synapse.[16] Pulses of light stimulated output voltage signals from the organic PD; they were applied to series-connected organic stretchable synaptic transistors to demonstrate a sensory nerve and generated postsynaptic responses. The postsynaptic electrical signals operated a polymer actuator, so an optoelectronic sensorimotor synapse was demonstrated.[16] This use of a self-powered photosensor in integrated systems reduced *E* to 1.8 nW in the "off" state and 2.8 nW in the "on" state, which correspond to the energy dissipated only by the synaptic device.[16]

Artificial synapses with self-powered elements[16,99,117] have an estimated average *E* in the microwatt range (Figure 4). It should be noted that the *E* depends on the application. To stimulate biological neurons in a prosthetic device, the *P* of the artificial synapses must be large (3 V × 100 μA = 300 μW).[118] However, applications for robots do not have such requirements on the output amplitude of the synaptic devices, so this is favorable in terms of low *E*.

Functional artificial synapses that combine sensing capabilities in a single device have been pursued because compactness without the requirement for additional sensing elements enables low *E* and high-density integration (Figure 4C).[119] These artificial sensory synapses have *P* in the microwatt range, which is comparable to that of artificial synapses that have self-powered sensing elements and lower than that of artificial synapses that have externally powered sensing elements (Figure 4). The human olfactory system has been emulated by a synaptic transistor that is sensitive to a hazardous gas (NO_2).[120] During exposure, NO_2 molecules were captured at the surface of the organic semiconductor layer and provided electron-trapping sites. The result was an increase in the number of holes that accumulated in the organic semiconductor layer and an increase in the current level in response to NO_2 gas exposure. This artificial NO_2-sensing synapse showed various synaptic properties depending on NO_2 exposure information.[120] A chemical-sensitive artificial synapse composed of PEDOT:PSS as electrodes can detect dopamine.[121] The sensing ability may be a result of attractive and repulsive forces between dopamine and PEDOT:PSS.[121] In addition, dopamine released from PC-12 cells into the cell culture media (an electrolyte) was detected at the PEDOT:PSS postsynaptic gate electrode due to the dopamine oxidation.[122] This dopamine oxidation was irreversible, so it yielded long-term potentiation (LTP) characteristics.[122] A pH-sensitive artificial synapse has also been reported; the mechanism may be a result of a decrease in the number of H^+ ions in PSS as the pH increases.[87] Tactile synaptic transistors have been demonstrated by using a pyramid-patterned ion gel or a nanocomposite ferroelectric polymer as the gate insulator.[98,109] In the case of the pyramid-patterned ion-gel gate insulator, when pressure was applied to the negatively biased top electrode, anions in the ion gel migrated into the organic polymer channel, poly(3-hexylthiophene-2,5-diyl), and the device showed synaptic properties.[98] In the synaptic transistor that used nanocomposite ferroelectric polymers as gate insulators, tactile stimuli induced dipole alignment in the ferroelectric gate insulator of PVDF-TrFE by triboelectric-capacitive coupling, so this device could emulate various synaptic properties in response to tactile information.[109] Photoactive organic memristors (2-T) and synaptic transistors (3-T) have been reported. Especially for 3-T devices, most of the photonic synapses exploit charge trapping

at the functional groups of gate insulators,[60,61] floating gates,[55,93,123] or additive nanomaterials[124]; these mechanisms require relatively high energy. *E* in all of these devices might be further reduced by adopting low-*E* mechanisms such as ion migration and redox reaction.

ENERGY CONSUMPTION OF ORGANIC NEUROMORPHIC PERIPHERAL SYSTEM

To replicate sensing and responding functions in biology, artificial synapses with sensing/motor functions are typically built in a von Neumann architecture that uses rigid silicon chips as sensing/motor units, decoders, analog multiplexers, and controllers.[10] Applications in human-like robots and neural prostheses would require a huge number of sensor/motor pixels. Each pixel requires periodic scanning, which wastes an enormous amount of energy, so the event-based operation of a neuromorphic system is advantageous for reducing energy dissipation.[10,125] Therefore, several researchers have attempted to develop neuromorphic systems that emulate the energy efficiency of biological nervous systems.

The systems demonstrated in Energy consumption of artificial synapses integrated with sensing/motor elements (the previous chapter) lack signal encoders such as ring oscillators (ROSCs)[65,74,89,101] and, therefore, cannot transform external stimuli to signal spikes. Instead, external stimuli such as light and pressure are applied directly to the systems in the limited form of spikes, but this method is not adequate for practical applications. Operations in the real world use various forms of stimuli in addition to spikes.

Pulse-frequency modulation is advantageous for low *E* because the method is relatively insensitive to noise interference so that the voltage amplitude is not required to be unnecessarily high.[126] Thus, signal transmission by use of voltage spikes is useful, especially for mechanically stretchable and flexible electronic systems in which noise from contact and wiring resistances varies severely during stretching and bending deformations.

ROSCs have been applied in a bio-inspired artificial mechanosensory system to convert external stimuli to frequency-modulated signals.[10] The goal of the study was to mimic the functions of biological mechanosensory nerves, i.e., to achieve bio-inspired artificial afferent nerves. In biology, pressure information from multiple mechanoreceptors is collected and transferred to synapses for information processing. Then, the processed information is conveyed to the efferent nerves to stimulate response by muscles to the external stimuli. The operating principle of the bio-inspired artificial afferent nervous systems is as follows. An artificial mechanoreceptor (a pressure sensor) was combined with an artificial nerve fiber (a ROSC) that converted pressure information to action potentials (voltage pulses). The voltage pulses from multiple artificial nerve fibers were integrated in a synaptic transistor for information processing.[10] A hybrid reflex arc was constructed by connecting fabricated artificial afferent nerves to biological motor nerves (muscles in a cockroach); the arc successfully actuated muscles in response to pressure information. This result verified the applicability of this approach to neuroprostheses.[10] Signals in biological systems are similar to voltage spikes, so use of voltage-spike encoding ensures biocompatibility of signal forms in prostheses.[127]

An array of organic artificial afferent nerves that emulate both the function and the structure of biological afferent nerves can be operated with lower *P* than required by a conventional sensory system which mimics only the function of biological

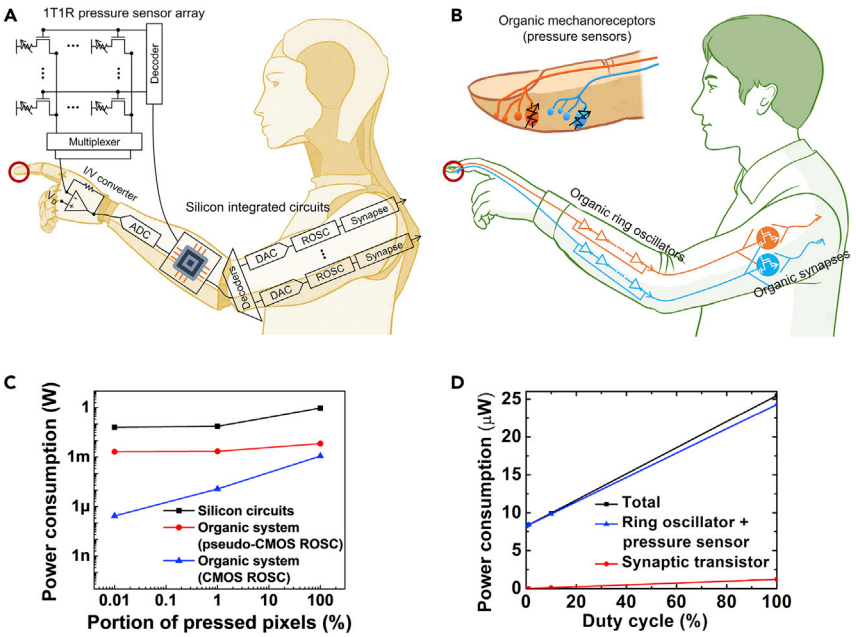

Figure 5. Comparisons between a conventional sensory system with silicon-integrated circuit chips and organic artificial afferent nerves

(A and B) System illustrations of (A) conventional sensory system that uses an 1-transistor/1-resistor pressure sensor array operated by silicon-integrated circuit chips (decoders, analog multiplexer, current-to-voltage converter, ADC, control chip, DACs, ROSCs, and synapses) and (B) an array of organic artificial afferent nerves with organic pressure sensors, organic ROSCs, and organic synaptic transistors connected in series.

(C) Comparison or power consumption by conventional sensory system with silicon circuits (black) and organic artificial afferent nerves with pseudo-CMOS ROSC (red) and with CMOS ROSC (blue).

(D) Power comparison of an organic artificial afferent nerve as a function of duty cycle. Reproduced with permission.[10] Copyright 2018, American Association for the Advancement of Science.

afferent nerves and is composed of 1-transistor/1-resistor sensor array and low-power silicon-integrated circuit chips (a decoder, an analog multiplexer, a current-to-voltage [I/V] converter, an analog-to-digital converter [ADC], a control chip, a digital-to-analog converter [DAC], a ROSC and a synapse; Figure 5A).[10] To detect electrical changes in stimulated pixels, the conventional system must periodically read and control all pixels; this continuous scanning of every pixel requires "idle" P, which increases the overall P. In contrast, organic artificial afferent nerves do not require external silicon-integrated readout and control circuit chips because each sensor pixel has its own individual output line in a manner similar to the structure of biological nerves (Figure 5B).[10] This sensing by artificial afferent nerves only in response to an event spends minimum standby power (Figure 5C) but needs a large number of output lines, so this architecture is not favorable for electronics and robotics. This also can be resolved by data preprocessing of artificial afferent nerves.

Although the organic system emulates the operating principles and signal forms of biological systems in a rather complete manner,[10] the P of each component can be further optimized. The combination of a pressure sensor and a ROSC consumed $8\ \mu W \leq P \leq 24\ \mu W$ depending on the duty cycle (the proportion of time that the pressure sensor is fully compressed), whereas a synaptic transistor consumed only $0.6\ nW \leq P \leq 1.2\ \mu W$, which is tiny compared to the requirements of sensing and signal-encoding elements (Figure 5D).[10]

As a strategy to reduce *P*, the types of ROSCs in the system can be optimized. More specifically, an ROSC that uses a pseudo-CMOS can be replaced with an ROSC that uses a CMOS. ROSCs that use a pseudo-CMOS that only uses monotype (p- or n-type) single-threshold voltage transistors have been widely investigated because the manufacturing process is inexpensive and simple.[128,129] However, CMOS-type ROSCs consume nanowatt-scale power, which is much less than that of ROSCs that use a pseudo-CMOS (Figure 5C).[128] The *P* was simulated with 3-stage CMOS organic ring oscillators.[130] However, actual application of CMOS type requires that several problems must be solved, including instability of n-type materials, mismatch in carrier mobility μ and V_{th} between n- and p-type devices, and complicated manufacturing processes.[128] *E* can be further reduced at the transistor level of ROSC components, and the methods include scaling down of device dimensions, reducing the energy barrier between organic semiconductors and source/drain electrodes, and using a gate insulator that has a high dielectric constant and organic semiconductors that have high μ.

CONCLUSIONS AND OUTLOOK

We have reviewed recent research related to organic neuromorphic electronics and have discussed how to reduce the *E* of organic artificial synapses and artificial nervous systems. Unlike silicon CMOS-based artificial synapses, which require complicated circuits and large *E* for successful emulation of biological synapses, organic artificial synapses have been developed to replicate biological synaptic functions by using straightforward operations and simple structures (2-T and 3-T devices). These devices are advantageous because of their (1) compatibility with solution-printing and micro-patterning lithography; (2) easy tunability of molecular, chemical, electrical, and mechanical properties for many purposes; and (3) mechanical flexibility/stretchability with low elastic modulus similar to those of soft biological systems. Therefore, organic neuromorphic electronics constitute promising candidates for next-generation computing devices, biomimetic robots, and neural prostheses.

At the level of an artificial synapse, *E* is simply proportional to applied voltage, drain current, and duration of the programming pulse. To minimize applied voltage, artificial synapses that exploit ion migration have a high EDL capacitance in electrolyte gate insulators, so these artificial synapses are preferred because they require only a low driving voltage. Active layers should be "normally OFF" because "normally ON" devices with relatively conductive active layers such as PEDOT:PSS exhibit high current states even before programming, so they use much more energy than "normally OFF" devices. Other options to reduce *E* are to decrease the duration of programming spikes and to scale down device size.

Artificial synapses integrated with sensing/motor functions should be developed to mimic complicated sensing/motor functions in biological systems for soft robotics and neural prosthetics. For these systems, synaptic characteristics must be integrated with sensing elements; three types of devices can be achieved: artificial synapses integrated with externally powered sensing elements, artificial synapses integrated with self-powered sensing elements, and artificial sensory synapses. Artificial sensory nervous systems that use externally powered sensing elements dissipate additional energy (microwatts to milliiwatts) from the sensing elements, which is much higher than that of typical synaptic devices. As a solution to reduce energy dissipation from sensing elements, artificial synapses have been integrated with self-powered sensing elements, so most of the energy is dissipated only by the synaptic devices. Another approach is to use artificial sensory synapses, that is, functional artificial synapses with sensing capabilities in a single device. In addition to low *P*, these artificial synapses have the advantage of being compatible

with high-density integration. That is, to reduce *E* in artificial sensory nervous systems, artificial synapses with self-powered sensing elements and artificial sensory synapses are preferred over artificial synapses that use externally powered sensing elements.

Our discussion of methods to achieve low *E* in organic neuromorphic electronics may guide development of a wide range of actual applications in humanoid robots, smart sensors in the internet of things (IoT) systems, bio-implantable neural prostheses, and cybernetic electronic devices. Combined with low-energy artificial synapses, robot systems can demonstrate sophisticated movement by consuming low energy like biological nervous systems. For advanced robots and human-like sensory electronics, environment-adaptable perception behaviors in biological systems can be emulated by adaptive organic devices with synaptic functions. For IoT systems, artificial synapses with sensing functions enable localized memory functions in every smart sensing device; this ability would eliminate the possibility that private data could be revealed, as is possible in central processing systems (e.g., cloud computing). Moreover, neuromorphic cognitive systems with local processing can process numerous data from surroundings and make decisions by themselves without sending a large amount of data to the central processing systems; the reduced amount of communication will reduce *E*.

The biocompatibility of organic materials will permit the use of organic artificial synapses in bio-implantable electronic devices, but depending on the application, they can be used in the form of hybrids with CMOS devices.

In addition, low-energy-consuming organic artificial synapses combined with highly efficient power sources (e.g., thermoelectrics and solar cells) will facilitate actual daily-life application of these neuromorphic electronic systems in the real world.

ACKNOWLEDGMENTS

This work was supported by the National Research Foundation of Korea (NRF) grant funded by the Korea government (Ministry of Science and ICT) (grant no. NRF-2016R1A3B1908431) and the Creative-Pioneering Researchers Program through Seoul National University (SNU).

REFERENCES

1. Wang, Z., Wang, L., Nagai, M., Xie, L., Yi, M., and Huang, W. (2017). Nanoionics-enabled memristive devices: strategies and materials for neuromorphic applications. Adv. Electron. Mater. *3*, 1600510.
2. An, H., Ehsan, M.A., Zhou, Z., and Yi, Y. (2017). Electrical modeling and analysis of 3D synaptic array using vertical RRAM structure. 2017 18th International Symposium on Quality Electronic Design (ISQED) (IEEE), pp. 1–6.
3. Schneider, D. (2018). U.S. supercomputing strikes back. IEEE Spectr. *55*, 52–53.
4. Poon, C.-S., and Zhou, K. (2011). Neuromorphic silicon neurons and large-scale neural networks: challenges and opportunities. Front. Neurosci. *5*, 108.
5. Xu, W., Min, S.-Y., Hwang, H., and Lee, T.-W. (2016). Organic core-sheath nanowire artificial synapses with femtojoule energy consumption. Sci. Adv. *2*, e1501326.
6. van de Burgt, Y., and Gkoupidenis, P. (2020). Organic materials and devices for brain-inspired computing: From artificial implementation to biophysical realism. MRS Bull. *45*, 631–640.
7. Lee, Y., and Lee, T.-W. (2019). Organic synapses for neuromorphic electronics: From brain-inspired computing to sensorimotor nervetronics. Acc. Chem. Res. *52*, 964–974.
8. van de Burgt, Y., Melianas, A., Keene, S.T., Malliaras, G., and Salleo, A. (2018). Organic electronics for neuromorphic computing. Nat. Electron. *1*, 386–397.
9. Koutsouras, D.A., Malliaras, G.G., and Gkoupidenis, P. (2018). Emulating homeoplasticity phenomena with organic electrochemical devices. MRS Commun. *8*, 493–497.
10. Kim, Y., Chortos, A., Xu, W., Liu, Y., Oh, J.Y., Son, D., Kang, J., Foudeh, A.M., Zhu, C., Lee, Y., et al. (2018). A bioinspired flexible organic artificial afferent nerve. Science *360*, 998–1003.
11. Davies, M., Srinivasa, N., Lin, T.-H., Chinya, G., Cao, Y., Choday, S.H., Dimou, G., Joshi, P., Imam, N., Jain, S., et al. (2018). Loihi: a neuromorphic manycore processor with On-Chip learning. IEEE Micro *38*, 82–99.
12. Liu, C., Bellec, G., Vogginger, B., Kappel, D., Partzsch, J., Neumärker, F., Höppner, S., Maass, W., Furber, S.B., Legenstein, R., et al. (2018). Memory-efficient deep learning on a SpiNNaker 2 prototype. Front. Neurosci. *12*, 840.
13. Merolla, P.A., Arthur, J.V., Alvarez-Icaza, R., Cassidy, A.S., Sawada, J., Akopyan, F., Jackson, B.L., Imam, N., Guo, C., Nakamura, Y., and Mayr, C.G. (2014). Artificial brains. A million spiking-neuron integrated circuit with a scalable communication network and interface. Science *345*, 668–673.
14. Park, H.-L., Lee, Y., Kim, N., Seo, D.-G., Go, G.-T., and Lee, T.-W. (2020). Flexible neuromorphic electronics for computing, soft robotics, and neuroprosthetics. Adv. Mater. *32*, e1903558.
15. Wan, C., Cai, P., Wang, M., Qian, Y., Huang, W., and Chen, X. (2020). Artificial sensory memory. Adv. Mater. *32*, e1902434.

16. Lee, Y., Oh, J.Y., Xu, W., Kim, O., Kim, T.R., Kang, J., Kim, Y., Son, D., Tok, J.B.-H., Park, M.J., et al. (2018). Stretchable organic optoelectronic sensorimotor synapse. Sci. Adv. *4*, eaat7387.

17. Karbalaei Akbari, M., and Zhuiykov, S. (2019). A bioinspired optoelectronically engineered artificial neurorobotics device with sensorimotor functionalities. Nat. Commun. *10*, 3873.

18. Shim, H., Sim, K., Ershad, F., Yang, P., Thukral, A., Rao, Z., Kim, H.-J.J., Liu, Y., Wang, X.X., Gu, G., et al. (2019). Stretchable elastic synaptic transistors for neurologically integrated soft engineering systems. Sci. Adv. *5*, eaax4961.

19. van Doremaele, E.R.W., Gkoupidenis, P., and van de Burgt, Y. (2019). Towards organic neuromorphic devices for adaptive sensing and novel computing paradigms in bioelectronics. J. Mater. Chem. C *7*, 12754–12760.

20. Lee, W.W., Tan, Y.J., Yao, H., Li, S., See, H.H., Hon, M., Ng, K.A., Xiong, B., Ho, J.S., and Tee, B.C.K. (2019). A neuro-inspired artificial peripheral nervous system for scalable electronic skins. Sci. Robot. *4*, eaax2198.

21. Rus, D., and Tolley, M.T. (2015). Design, fabrication and control of soft robots. Nature *521*, 467–475.

22. Laschi, C., Mazzolai, B., and Cianchetti, M. (2016). Soft robotics: technologies and systems pushing the boundaries of robot abilities. Sci. Robot. *1*, eaah3690.

23. Nawrocki, R.A., Voyles, R.M., and Shaheen, S.E. (2016). A mini review of neuromorphic architectures and implementations. IEEE Trans. Electron Devices *63*, 3819–3829.

24. Qiao, N., Mostafa, H., Corradi, F., Osswald, M., Stefanini, F., Sumislawska, D., and Indiveri, G. (2015). A reconfigurable on-line learning spiking neuromorphic processor comprising 256 neurons and 128K synapses. Front. Neurosci. *9*, 141.

25. Indiveri, G., Linares-Barranco, B., Hamilton, T.J., van Schaik, A., Etienne-Cummings, R., Delbruck, T., Liu, S.C., Dudek, P., Häfliger, P., Renaud, S., et al. (2011). Neuromorphic silicon neuron circuits. Front. Neurosci. *5*, 73.

26. Ishii, M., Kim, S., Lewis, S., Okazaki, A., Okazawa, J., Ito, M., Rasch, M., Kim, W., Nomura, A., Shin, U., et al. (2019). On-chip trainable 1.4M 6T2R PCM synaptic array with 1.6K stochastic LIF neurons for spiking RBM. 2019 IEEE International Electron Devices Meeting (IEDM) (IEEE), pp. 14.2.1–14.2.4.

27. Benjamin, B.V., Gao, P., McQuinn, E., Choudhary, S., Chandrasekaran, A.R., Bussat, J.-M., Alvarez-Icaza, R., Arthur, J.V., Merolla, P.A., and Boahen, K. (2014). Neurogrid: a mixed-analog-digital multichip system for large-scale neural simulations. Proc. IEEE *102*, 699–716.

28. Rajendran, B., Sebastian, A., Schmuker, M., Srinivasa, N., and Eleftheriou, E. (2019). Low-power neuromorphic hardware for signal processing applications: a review of architectural and system-level design approaches. IEEE Signal Process. Mag. *36*, 97–110.

29. Furber, S. (2016). Large-scale neuromorphic computing systems. J. Neural Eng. *13*, 051001.

30. Zhang, X., Huang, A., Hu, Q., Xiao, Z., and Chu, P.K. (2018). Neuromorphic computing with memristor crossbar. Phys. Status Solidi A *215*, 1700875.

31. Fonseca Guerra, G.A., and Furber, S.B. (2017). Using stochastic spiking neural networks on SpiNNaker to solve constraint satisfaction problems. Front. Neurosci. *11*, 714.

32. Knight, J.C., and Furber, S.B. (2016). Synapse-centric mapping of cortical models to the SpiNNaker neuromorphic architecture. Front. Neurosci. *10*, 420.

33. Furber, S.B., Galluppi, F., Temple, S., and Plana, L.A. (2014). The SpiNNaker project. Proc. IEEE *102*, 652–665.

34. Jeong, D.S., and Hwang, C.S. (2018). Nonvolatile memory materials for neuromorphic intelligent machines. Adv. Mater. *30*, e1704729.

35. Sun, J., Fu, Y., and Wan, Q. (2018). Organic synaptic devices for neuromorphic systems. J. Phys. D Appl. Phys. *51*, 314004.

36. Yu, F., and Zhu, L.Q. (2019). Ionotronic neuromorphic devices for bionic neural network applications. Phys. Status Solidi Rapid Res. Lett. *13*, 1800674.

37. van de Burgt, Y., Lubberman, E., Fuller, E.J., Keene, S.T., Faria, G.C., Agarwal, S., Marinella, M.J., Alec Talin, A., and Salleo, A. (2017). A non-volatile organic electrochemical device as a low-voltage artificial synapse for neuromorphic computing. Nat. Mater. *16*, 414–418.

38. Gkoupidenis, P., Koutsouras, D.A., and Malliaras, G.G. (2017). Neuromorphic device architectures with global connectivity through electrolyte gating. Nat. Commun. *8*, 15448.

39. Pereda, A.E. (2014). Electrical synapses and their functional interactions with chemical synapses. Nat. Rev. Neurosci. *15*, 250–263.

40. Connors, B.W., and Long, M.A. (2004). Electrical synapses in the mammalian brain. Annu. Rev. Neurosci. *27*, 393–418.

41. Sandberg, A. (2016). Energetics of the brain and AI. arXiv, arXiv:1602.04019.

42. John, R.A., Tiwari, N., Yaoyi, C., Ankit, Tiwari, N., Kulkarni, M., Nirmal, A., Nguyen, A.C., Basu, A., and Mathews, N. (2018). Ultralow power dual-gated subthreshold oxide Neuristors: an enabler for higher order neuronal temporal correlations. ACS Nano *12*, 11263–11273.

43. Zhao, J., Zhou, Z., Zhang, Y., Wang, J., Zhang, L., Li, X., Zhao, M., Wang, H., Pei, Y., Zhao, Q., et al. (2019). An electronic synapse memristor device with conductance linearity using quantized conduction for neuroinspired computing. J. Mater. Chem. C *7*, 1298–1306.

44. Park, Y., and Lee, J.-S. (2017). Artificial synapses with short- and long-term memory for spiking neural networks based on renewable materials. ACS Nano *11*, 8962–8969.

45. Li, S., Zeng, F., Chen, C., Liu, H., Tang, G., Gao, S., Song, C., Lin, Y., Pan, F., and Guo, D. (2013). Synaptic plasticity and learning behaviours mimicked through Ag interface movement in an Ag/conducting polymer/Ta memristive system. J. Mater. Chem. C *1*, 5292–5298.

46. Kim, M.-K., and Lee, J.-S. (2018). Short-term plasticity and long-term potentiation in artificial biosynapses with diffusive dynamics. ACS Nano *12*, 1680–1687.

47. Lee, S.-H., Park, H.-L., Keum, C.-M., Lee, I.-H., Kim, M.-H., and Lee, S.-D. (2019). Organic flexible memristor with reduced operating voltage and high stability by interfacial control of conductive filament growth. Phys. Status Solidi RRL *13*, 1900044.

48. Lee, S.-H., Park, H.-L., Kim, M.-H., Kang, S., and Lee, S.-D. (2019). Interfacial triggering of conductive filament growth in organic flexible memristor for high reliability and uniformity. ACS Appl. Mater. Interfaces *11*, 30108–30115.

49. Shi, C., Lan, J., Wang, J., Zhang, S., Lin, Y., Zhu, S., Stegmann, A.E., Yu, R., Yan, X., and Liu, X.Y. (2020). Flexible and insoluble artificial synapses based on chemical cross-linked wool keratin. Adv. Funct. Mater. *30*, 2002882.

50. Jang, B.C., Kim, S., Yang, S.Y., Park, J., Cha, J.-H., Oh, J., et al. (2019). Polymer analog memristive synapse with atomic-scale conductive filament for flexible neuromorphic computing system. Nano Lett. *19*, 839–849.

51. Ge, J., Li, D., Huang, C., Zhao, X., Qin, J., Liu, H., Ye, W., Xu, W., Liu, Z., and Pan, S. (2020). Memristive synapses with high reproducibility for flexible neuromorphic networks based on biological nanocomposites. Nanoscale *12*, 720–730.

52. Yang, M., Zhao, X., Tang, Q., Cui, N., Wang, Z., Tong, Y., and Liu, Y. (2018). Stretchable and conformable synapse memristors for wearable and implantable electronics. Nanoscale *10*, 18135–18144.

53. Kim, C.-H., Sung, S., and Yoon, M.-H. (2016). Synaptic organic transistors with a vacuum-deposited charge-trapping nanosheet. Sci. Rep. *6*, 33355.

54. Ren, Y., Yang, J.Q., Zhou, L., Mao, J.Y., Zhang, S.R., Zhou, Y., and Han, S.T. (2018). Gate-tunable synaptic plasticity through controlled polarity of charge trapping in fullerene composites. Adv. Funct. Mater. *28*, 1805599.

55. Wang, Y., Lv, Z., Chen, J., Wang, Z., Zhou, Y., Zhou, L., Chen, X., and Han, S.T. (2018). Photonic synapses based on inorganic perovskite quantum dots for neuromorphic computing. Adv. Mater. *30*, e1802883.

56. Kwon, K.-C., Lee, J.-S., Kim, C.G., and Park, J.-G. (2013). Biological synapse behavior of nanoparticle organic memory field effect transistor fabricated by curing. Appl. Phys. Express *6*, 067001.

57. Alibart, F., Pleutin, S., Guérin, D., Novembre, C., Lenfant, S., Lmimouni, K., Gamrat, C., and Vuillaume, D. (2010). An organic nanoparticle transistor behaving as a biological spiking synapse. Adv. Funct. Mater. *20*, 330–337.

58. Desbief, S., Kyndiah, A., Guérin, D., Gentili, D., Murgia, M., Lenfant, S., Alibart, F., Cramer, T., Biscarini, F., and Vuillaume, D. (2015). Low

voltage and time constant organic synapse-transistor. Org. Electron. *21*, 47–53.

59. Desbief, S., di Lauro, M., Casalini, S., Guerin, D., Tortorella, S., Barbalinardo, M., Kyndiah, A., Murgia, M., Cramer, T., Biscarini, F., and Vuillaume, D. (2016). Electrolyte-gated organic synapse transistor interfaced with neurons. Org. Electron. *38*, 21–28.

60. Dai, S., Wu, X., Liu, D., Chu, Y., Wang, K., Yang, B., and Huang, J. (2018). Light-stimulated synaptic devices utilizing interfacial effect of organic field-effect transistors. ACS Appl. Mater. Interfaces *10*, 21472–21480.

61. Wu, X., Chu, Y., Liu, R., Katz, H.E., and Huang, J. (2017). Pursuing polymer dielectric interfacial effect in organic transistors for photosensing performance optimization. Adv. Sci. *4*, 1700442.

62. Hwang, S.K., Park, T.J., Kim, K.L., Cho, S.M., Jeong, B.J., and Park, C. (2014). Organic one-transistor-type nonvolatile memory gated with thin ionic liquid-polymer film for low voltage operation. ACS Appl. Mater. Interfaces *6*, 20179–20187.

63. Hwang, S.K., Min, S.-Y., Bae, I., Cho, S.M., Kim, K.L., Lee, T.-W., et al. (2014). Non-volatile ferroelectric memory with position-addressable polymer semiconducting nanowire. Small *10*, 1976–1984.

64. Hwang, S.K., Bae, I., Kim, R.H., and Park, C. (2012). Flexible non-volatile ferroelectric polymer memory with gate-controlled multilevel operation. Adv. Mater. *24*, 5910–5914.

65. Wang, H., Zhao, Q., Ni, Z., Li, Q., Liu, H., Yang, Y., Wang, L., Ran, Y., Guo, Y., Hu, W., and Liu, Y. (2018). A ferroelectric/electrochemical modulated organic synapse for ultraflexible, artificial visual-perception system. Adv. Mater. *30*, e1803961.

66. Jang, S., Jang, S., Lee, E.-H., Kang, M., Wang, G., and Kim, T.-W. (2019). Ultrathin conformable organic artificial synapse for wearable intelligent device applications. ACS Appl. Mater. Interfaces *11*, 1071–1080.

67. Kong, L.-A., Sun, J., Qian, C., Fu, Y., Wang, J., Yang, J., and Gao, Y. (2017). Long-term synaptic plasticity simulated in ionic liquid/polymer hybrid electrolyte gated organic transistors. Org. Electron. *47*, 126–132.

68. John, R.A., Liu, F., Chien, N.A., Kulkarni, M.R., Zhu, C., Fu, Q., Basu, A., Liu, Z., and Mathews, N. (2018). Synergistic gating of electro-iono-photoactive 2D chalcogenide Neuristors: coexistence of Hebbian and homeostatic synaptic metaplasticity. Adv. Mater. *30*, e1800220.

69. Gkoupidenis, P., Schaefer, N., Garlan, B., and Malliaras, G.G. (2015). Neuromorphic functions in PEDOT:PSS organic electrochemical transistors. Adv. Mater. *27*, 7176–7180.

70. Yang, J.J., and Xia, Q. (2017). Organic electronics: battery-like artificial synapses. Nat. Mater. *16*, 396–397.

71. Duong, D.T., Tuchman, Y., Chakthranont, P., Cavassin, P., Colucci, R., Jaramillo, T.F., Salleo, A., and Faria, G.C. (2018). A universal platform for fabricating organic electrochemical devices. Adv. Electron. Mater. *4*, 1800090.

72. Keene, S.T., Melianas, A., Fuller, E.J., van de Burgt, Y., Talin, A.A., and Salleo, A. (2018). Optimized pulsed write schemes improve linearity and write speed for low-power organic neuromorphic devices. J. Phys. D: Appl. Phys. *51*, 224002.

73. Wang, X., Zhou, Z., Ban, C., Zhang, Z., Ju, S., Huang, X., et al. (2020). Multifunctional polymer memory via bi-interfacial topography for pressure perception recognition. Adv. Sci. *7*, 1902864.

74. Ge, J., Zhang, S., Liu, Z., Xie, Z., and Pan, S. (2019). Flexible artificial nociceptor using a biopolymer-based forming-free memristor. Nanoscale *11*, 6591–6601.

75. Mao, J.-Y., Zhou, L., Ren, Y., Yang, J.-Q., Chang, C.-L., Lin, H.-C., Chou, H.-H., Zhang, S.-R., Zhou, Y., and Han, S.-T. (2019). A bio-inspired electronic synapse using solution processable organic small molecule. J. Mater. Chem. C *7*, 1491–1501.

76. Wang, L., Yang, J., Zhu, Y., Yi, M., Xie, L., Ju, R., Wang, Z., Liu, L., Li, T., Zhang, C., et al. (2017). Rectification-regulated memristive characteristics in electron-type CuPc-based element for electrical synapse. Adv. Electron. Mater. *3*, 1700063.

77. Zhou, L., Zhang, S.R., Yang, J.Q., Mao, J.Y., Ren, Y., Shan, H., Xu, Z., Zhou, Y., and Han, S.T. (2020). A UV damage-sensing nociceptive device for bionic applications. Nanoscale *12*, 1484–1494.

78. Sung, S., Park, J.H., Wu, C., and Kim, T.W. (2020). Biosynaptic devices based on chicken egg albumen:graphene quantum dot nanocomposites. Sci. Rep. *10*, 1255.

79. Zhong, Y.-N., Wang, T., Gao, X., Xu, J.-L., and Wang, S.-D. (2018). Synapse-like organic thin film memristors. Adv. Funct. Mater. *28*, 1800854.

80. Ren, Y., Chang, C.-L., Ting, L.-Y., Zhou, L., Mao, J.-Y., Zhang, S.-R., Chou, H.-H., Yang, J.-Q., Zhou, Y., and Han, S.-T. (2019). Flexible pyrene/phenanthro[9,10-d]imidazole-based memristive devices for mimicking synaptic plasticity. Adv. Intell. Syst. *1*, 1900008.

81. Liu, G., Wang, C., Zhang, W., Pan, L., Zhang, C., Yang, X., Fan, F., Chen, Y., and Li, R.-W. (2016). Organic biomimicking memristor for information storage and processing applications. Adv. Electron. Mater. *2*, 1500298.

82. Zhang, C., Tai, Y.-T., Shang, J., Liu, G., Wang, K.-L., Hsu, C., Yi, X., Yang, X., Xue, W., Tan, H., et al. (2016). Synaptic plasticity and learning behaviours in flexible artificial synapse based on polymer/viologen system. J. Mater. Chem. C *4*, 3217–3223.

83. Zeng, F., Lu, S., Li, S., Li, X., and Pan, F. (2014). Frequency selectivity in pulse responses of Pt/poly(3-hexylthiophene-2,5-diyl)/polyethylene oxide + Li+/Pt hetero-junction. PLoS One *9*, e108316.

84. Yang, X., Wang, C., Shang, J., Zhang, C., Tan, H., Yi, X., et al. (2016). An organic terpyridyl-iron polymer based memristor for synaptic plasticity and learning behavior simulation. RSC Adv. *6*, 25179–25184.

85. Xiao, Z., and Huang, J. (2016). Energy-efficient hybrid perovskite memristors and synaptic devices. Adv. Electron. Mater. *2*, 1600100.

86. Raeis-Hosseini, N., Park, Y., and Lee, J.-S. (2018). Flexible artificial synaptic devices based on collagen from fish protein with spike-timing-dependent plasticity. Adv. Funct. Mater. *28*, 1800553.

87. Zhao, Y., Dai, S., Chu, Y., Wu, X., and Huang, J. (2018). A flexible ionic synaptic device and diode-based aqueous ion sensor utilizing asymmetric polyelectrolyte distribution. Chem. Commun. *54*, 8186–8189.

88. Dong, W.S., Zeng, F., Lu, S.H., Liu, A., Li, X.J., and Pan, F. (2015). Frequency-dependent learning achieved using semiconducting polymer/electrolyte composite cells. Nanoscale *7*, 16880–16889.

89. Zhang, C., Ye, W.B., Zhou, K., Chen, H., Yang, J., Ding, G., Chen, X., Zhou, Y., Zhou, L., Li, F., and amd Han, S.-T. (2019). Bioinspired artificial sensory nerve based on nafion memristor. Adv. Funct. Mater. *29*, 1808783.

90. Wu, C., Kim, T.W., Choi, H.Y., Strukov, D.B., and Yang, J.J. (2017). Flexible three-dimensional artificial synapse networks with correlated learning and trainable memory capability. Nat. Commun. *8*, 752.

91. Xu, W., Cho, H., Kim, Y.-H., Kim, Y.-T., Wolf, C., Park, C.-G., et al. (2016). Organometal halide perovskite artificial synapses. Adv. Mater. *28*, 5916–5922.

92. Xu, W., Nguyen, T.L., Kim, Y.-T., Wolf, C., Pfattner, R., Lopez, J., Chae, B.-G., Kim, S.-I., Lee, M.Y., Shin, E.-Y., et al. (2018). Ultrasensitive artificial synapse based on conjugated polyelectrolyte. Nano Energy *48*, 575–581.

93. Mao, J.-Y., Hu, L., Zhang, S.-R., Ren, Y., Yang, J.-Q., Zhou, L., Zeng, Y.-J., Zhou, Y., and Han, S.-T. (2019). Artificial synapses emulated through a light mediated organic–inorganic hybrid transistor. J. Mater. Chem. C *7*, 48–59.

94. Wang, Y., Liao, Q., She, D., Lv, Z., Gong, Y., Ding, G., Ye, W., Chen, J., Xiong, Z., Wang, G., et al. (2020). Modulation of binary neuroplasticity in a heterojunction-based ambipolar transistor. ACS Appl. Mater. Interfaces *12*, 15370–15379.

95. Alibart, F., Pleutin, S., Bichler, O., Gamrat, C., Serrano-Gotarredona, T., Linares-Barranco, B., and Vuillaume, D. (2012). A memristive nanoparticle/organic hybrid synapstor for neuroinspired computing. Adv. Funct. Mater. *22*, 609–616.

96. Yu, R., Li, E., Wu, X., Yan, Y., He, W., He, L., Chen, J., Chen, H., and Guo, T. (2020). Electret-based organic synaptic transistor for neuromorphic computing. ACS Appl. Mater. Interfaces *12*, 15446–15455.

97. Lyu, B., Choi, Y., Jing, H., Qian, C., Kang, H., Lee, S., and Cho, J.H. (2020). 2D MXene–TiO2 core–shell nanosheets as a data-storage medium in memory devices. Adv. Mater. *32*, e1907633.

98. Kim, D.W., Yang, J.C., Lee, S., and Park, S. (2020). Neuromorphic processing of pressure signal using integrated sensor-synaptic device capable of selective and reversible short- and long-term plasticity operation. ACS Appl. Mater. Interfaces *12*, 23207–23216.

99. Liu, Y., Zhong, J., Li, E., Yang, H., Wang, X., Lai, D., Chen, H., and Guo, T. (2019). Self-powered artificial synapses actuated by triboelectric nanogenerator. Nano Energy *60*, 377–384.

100. Wang, X., Yan, Y., Li, E., Liu, Y., Lai, D., Lin, Z., Liu, Y., Chen, H., and Guo, T. (2020). Stretchable synaptic transistors with tunable synaptic behavior. Nano Energy *75*, 104952.

101. Zang, Y., Shen, H., Huang, D., Di, C.A., and Zhu, D. (2017). A dual-organic-transistor-based tactile-perception system with signal-processing functionality. Adv. Mater. *29*, 1606088.

102. Qian, C., Sun, J., Kong, L.A., Gou, G., Yang, J., He, J., Gao, Y., and Wan, Q. (2016). Artificial Synapses based on in-plane gate organic electrochemical transistors. ACS Appl. Mater. Interfaces *8*, 26169–26175.

103. Lenz, J., del Giudice, F., Geisenhof, F.R., Winterer, F., and Weitz, R.T. (2019). Vertical, electrolyte-gated organic transistors show continuous operation in the MA cm−2 regime and artificial synaptic behaviour. Nat. Nanotechnol. *14*, 579–585.

104. Feng, P., Xu, W., Yang, Y., Wan, X., Shi, Y., Wan, Q., Zhao, J., and Cui, Z. (2017). Printed neuromorphic devices based on printed carbon nanotube thin-film transistors. Adv. Funct. Mater. *27*, 1604447.

105. Liu, D., Shi, Q., Dai, S., and Huang, J. (2020). The design of 3D-interface architecture in an ultralow-power, electrospun single-fiber synaptic transistor for neuromorphic computing. Small *16*, e1907472.

106. Liu, Q., Liu, Y., Li, J., Lau, C., Wu, F., Zhang, A., Li, Z., Chen, M., Fu, H., Draper, J., et al. (2019). Fully printed all-solid-state organic flexible artificial synapse for neuromorphic computing. ACS Appl. Mater. Interfaces *11*, 16749–16757.

107. Ling, H., Wang, N., Yang, A., Liu, Y., Song, J., and Yan, F. (2019). Dynamically reconfigurable short-term synapse with millivolt stimulus resolution based on organic electrochemical transistors. Adv. Mater. Technol. *4*, 1900471.

108. Fuller, E.J., Keene, S.T., Melianas, A., Wang, Z., Agarwal, S., Li, Y., Tuchman, Y., James, C.D., Marinella, M.J., Yang, J.J., et al. (2019). Parallel programming of an ionic floating-gate memory array for scalable neuromorphic computing. Science *364*, 570–574.

109. Lee, Y.R., Trung, T.Q., Hwang, B.-U., and Lee, N.-E. (2020). A flexible artificial intrinsic-synaptic tactile sensory organ. Nat. Commun. *11*, 2753.

110. Ham, S., Kang, M., Jang, S., Jang, J., Choi, S., Kim, T.W., and Wang, G. (2020). One-dimensional organic artificial multi-synapses enabling electronic textile neural network for wearable neuromorphic applications. Sci. Adv. *6*, eaba1178.

111. Kaltenbrunner, M., Sekitani, T., Reeder, J., Yokota, T., Kuribara, K., Tokuhara, T., Drack, M., Schwödiauer, R., Graz, I., Bauer-Gogonea, S., et al. (2013). An ultra-lightweight design for imperceptible plastic electronics. Nature *499*, 458–463.

112. Takei, K., Takahashi, T., Ho, J.C., Ko, H., Gillies, A.G., Leu, P.W., Fearing, R.S., and Javey, A. (2010). Nanowire active-matrix circuitry for low-voltage macroscale artificial skin. Nat. Mater. *9*, 821–826.

113. Schwartz, G., Tee, B.C.-K., Mei, J., Appleton, A.L., Kim, D.H., Wang, H., and Bao, Z. (2013). Flexible polymer transistors with high pressure sensitivity for application in electronic skin and health monitoring. Nat. Commun. *4*, 1859.

114. Choong, C.L., Shim, M.B., Lee, B.S., Jeon, S., Ko, D.S., Kang, T.H., Bae, J., Lee, S.H., Byun, K.E., Im, J., et al. (2014). Highly stretchable resistive pressure sensors using a conductive elastomeric composite on a micropyramid array. Adv. Mater. *26*, 3451–3458.

115. Park, J., Lee, Y., Hong, J., Ha, M., Jung, Y.D., Lim, H., Kim, S.Y., and Ko, H. (2014). Giant tunneling piezoresistance of composite elastomers with interlocked microdome arrays for ultrasensitive and multimodal electronic skins. ACS Nano *8*, 4689–4697.

116. Gong, S., Schwalb, W., Wang, Y., Chen, Y., Tang, Y., Si, J., Shirinzadeh, B., and Cheng, W. (2014). A wearable and highly sensitive pressure sensor with ultrathin gold nanowires. Nat. Commun. *5*, 3132.

117. Seo, D.-G., Lee, Y., Go, G.-T., Pei, M., Jung, S., Jeong, Y.H., et al. (2019). Versatile neuromorphic electronics by modulating synaptic decay of single organic synaptic transistor: from artificial neural networks to neuro-prosthetics. Nano Energy *65*, 104035.

118. Hughes, G.M. (1952). Differential effects of direct current on insect ganglia. J. Exp. Biol. *29*, 387–402.

119. Seo, S., Jo, S.H., Kim, S., Shim, J., Oh, S., Kim, J.H., Heo, K., Choi, J.W., Choi, C., Oh, S., et al. (2018). Artificial optic-neural synapse for colored and color-mixed pattern recognition. Nat. Commun. *9*, 5106.

120. Song, Z., Tong, Y., Zhao, X., Ren, H., Tang, Q., and Liu, Y. (2019). A flexible conformable artificial organ-damage memory system towards hazardous gas leakage based on a single organic transistor. Mater. Horiz. *6*, 717–726.

121. Giordani, M., Berto, M., Di Lauro, M., Bortolotti, C.A., Zoli, M., and Biscarini, F. (2017). Specific dopamine sensing based on short-term plasticity behavior of a whole organic artificial synapse. ACS Sens *2*, 1756–1760.

122. Keene, S.T., Lubrano, C., Kazemzadeh, S., Melianas, A., Tuchman, Y., Polino, G., Scognamiglio, P., Cinà, L., Salleo, A., van de Burgt, Y., and Santoro, F. (2020). A biohybrid synapse with neurotransmitter-mediated plasticity. Nat. Mater. *19*, 969–973.

123. Park, H.-L., Kim, H., Lim, D., Zhou, H., Kim, Y.-H., Lee, Y., et al. (2020). Retina-inspired carbon nitride-based photonic synapses for selective detection of UV light. Adv. Mater. *32*, e1906899.

124. Wang, K., Dai, S., Zhao, Y., Wang, Y., Liu, C., and Huang, J. (2019). Light-stimulated synaptic transistors fabricated by a facile solution process based on inorganic perovskite quantum dots and organic semiconductors. Small *15*, e1900010.

125. Liu, S.C., and Delbruck, T. (2010). Neuromorphic sensory systems. Curr. Opin. Neurobiol. *20*, 288–295.

126. Murray, A.F., Del Corso, D., and Tarassenko, L. (1991). Pulse-stream VLSI neural networks mixing analog and digital techniques. IEEE Trans. Neural Netw. *2*, 193–204.

127. Bengtsson, F., Brasselet, R., Johansson, R.S., Arleo, A., and Jörntell, H. (2013). Integration of sensory quanta in cuneate nucleus neurons in vivo. PLoS One *8*, e56630.

128. Huang, T.-C., Fukuda, K., Lo, C.-M., Yeh, Y.-H., Sekitani, T., Someya, T., and Cheng, K.-T. (2011). Pseudo-CMOS: a design style for low-cost and robust flexible electronics. IEEE Trans. Electron Devices *58*, 141–150.

129. Shiwaku, R., Matsui, H., Nagamine, K., Uematsu, M., Mano, T., Maruyama, Y., Nomura, A., Tsuchiya, K., Hayasaka, K., Takeda, Y., et al. (2018). A printed organic circuit system for wearable amperometric electrochemical sensors. Sci. Rep. *8*, 6368.

130. Yokota, T., Nakagawa, T., Sekitani, T., Noguchi, Y., Fukuda, K., Zschieschang, U., Klauk, H., Takeuchi, K., Takamiya, M., Sakurai, T., and Someya, T. (2011). Control of threshold voltage in low-voltage organic complementary inverter circuits with floating gate structures. Appl. Phys. Lett. *98*, 193302.